Electronic Supplementary Material (ESI) for Journal of Materials Chemistry A.

Synergetic Enhancement of Energy Harvesting Performance in Triboelectric Nanogenerator using Ferroelectric Polarization for Self-Powered IR Signaling and Body Activity Monitoring

Manisha Sahu†, Venkateswaran Vivekananthan†, Sugato Hajra, Abisegapriyan K S, Nirmal Prashanth Maria Joseph Raj and Sang-Jae Kim*

Nanomaterials and System Lab, Faculty of Applied Energy Systems, Major of Mechatronics Engineering, Jeju National University, Jeju, 632-43 South Korea

Mailing address:

Prof. Sang-Jae Kim*, Manisha Sahu†, Venkateswaran Vivekananthan†, Sugato Hajra, Abisegapriyan K S, Nirmal Prashanth Maria Joseph Raj

Nanomaterials & System Lab, Department of Mechatronics Engineering,

Engineering Building No 4, D-130,

Jeju National University, Ara-1-Dong, Jeju-Si, Jeju-Do

Jeju-63243, South Korea.

Email Id: kimsangj@jejunu.ac.kr, manishasahu@jejunu.ac.kr, vivek@jejunu.ac.kr, sugatofl@jejunu.ac.kr

*Corresponding author (**Prof. Sang-Jae Kim**)

Figure S1: (a) Digital picture of the M-HG device, (b) bendable BCZT-BH6/PDMS CF, (c) stretchable BCZT-BH6/PDMS CF

Figure S2: Working mechanism of piezoelectric nanogenerator

Figure S3: Working mechanism of triboelectric nanogenerator

Figure S4: P-E loop of the (a) BCZT, (b) BCZT-BH2, (c) BCZT-BH4, (d) BCZT-8, (e) BCZT-BH10

Figure S5: Surface morphology of (a) BCZT, (b) BCZT-BH2, (c) BCZT-BH4, (d) BCZT-8, (e) BCZT-BH10

Figure S6: (a) Plain PDMS (b) 3 wt% particle loading (c) 5 wt% particle loading (d) 10 wt% particle loading and (e) 15 wt% particle loading

Figure S7: Frequency dependent (a) dielectric constant, (b) dielectric loss and (c) rietveld analysis of the BCZT-BH6 sample confirming the presence of combine phases (orthorhombic and tetragonal)

Figure S8: (a) The switching polarity test of the poled PNG-3 device, (b) The voltage output of the unpoled PNG-3 device at different acceleration, (c) The results of the operational stability test during 1600 sec of the M-HG device, (d) The equivalent circuit of the capacitor charging, (e) The energy stored by the 1 μF capacitor by PENG, TENG and hybrid device.

Figure S9: Voltage peak pattern of MS-HG during contact and separation upon body activity (bridge pose)

Table S1: Comparison of Remnant polarization in the prepared BCZT ceramics with various doping concentrations

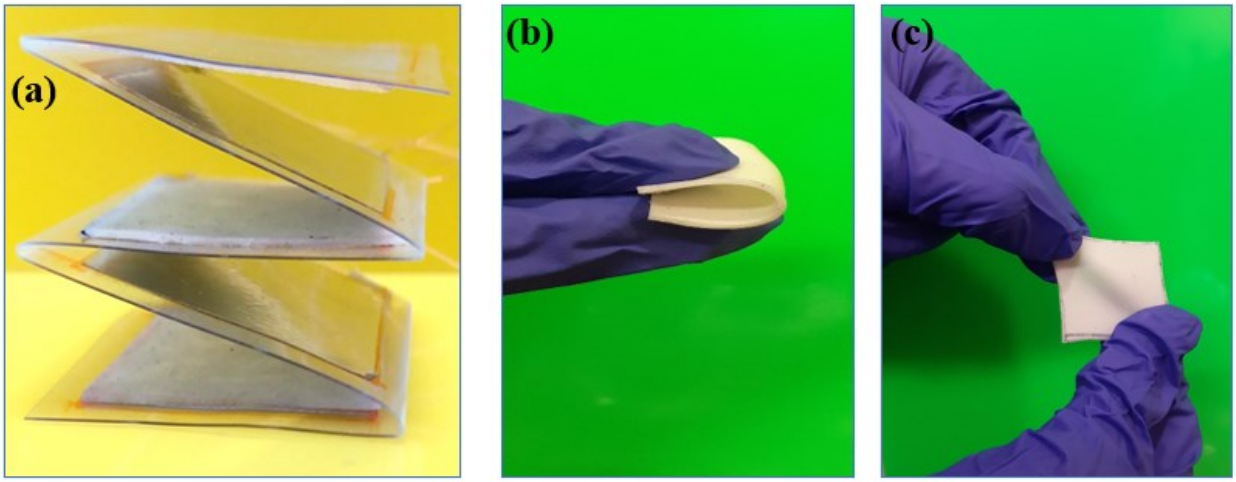

Figure S1: (a) Digital picture of the M-HG device, (b) bendable BCZT-BH6/PDMS CF, (c) stretchable BCZT-BH6/PDMS CF

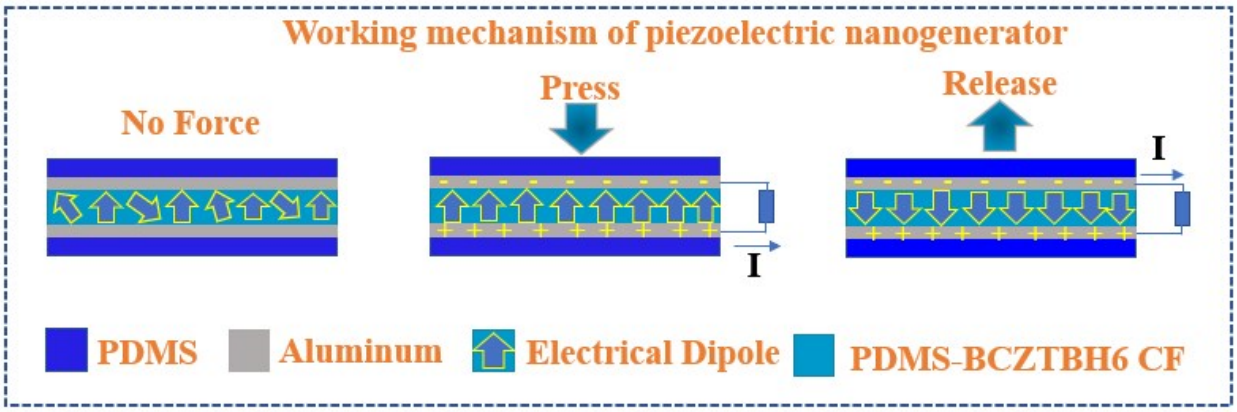

Figure S2: Working mechanism of piezoelectric nanogenerator

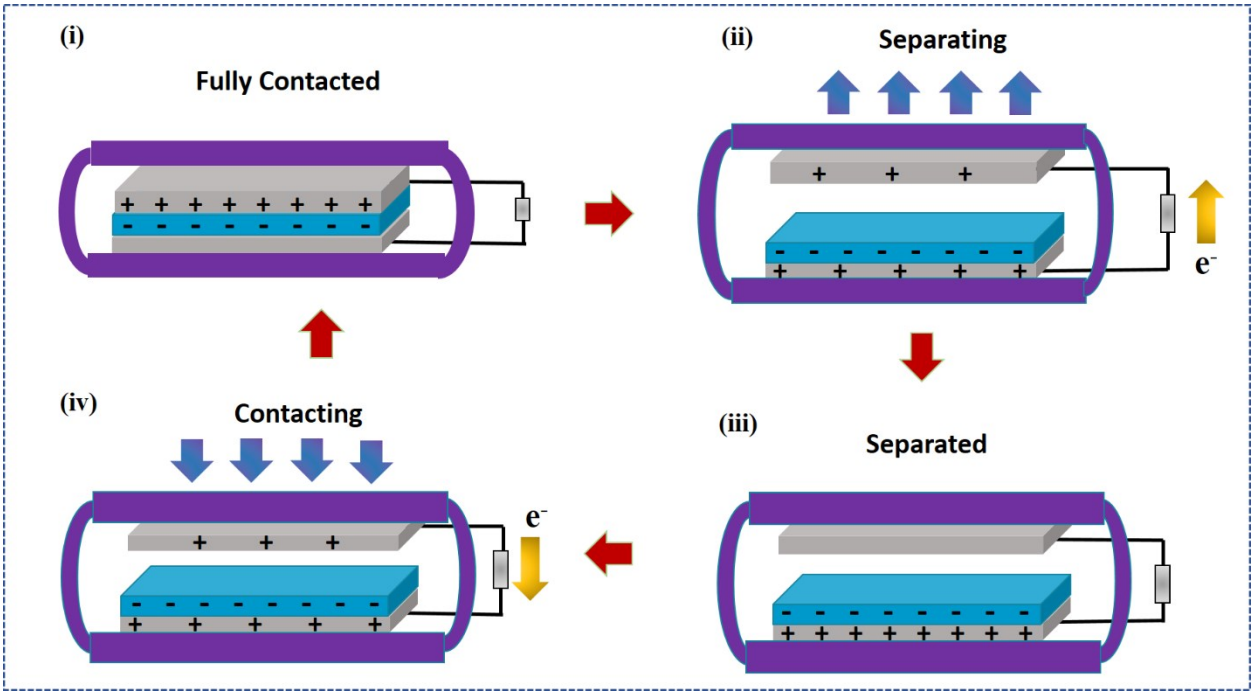

Figure S3: Working mechanism of triboelectric nanogenerator

The mechanism of triboelectric nanogenerator is schematically shown in Figure S3. (i) When the device is pressed the contact materials PDMS film and aluminum comes into contact, and the equal amount of opposite charges distributed on their contact surfaces due to coupling of triboelectrification and electrostatic induction. (ii) When the pressure slowly released from the device, the free electrons will migrate from bottom electrode to top electrode for balancing the potential difference until the space recovered. (iii) When the force is completely released, the charge distribution reaches an electrical equilibrium with no flow of electrons. (iv) When the top layer again comes into contact, the free electrons flow from top to bottom until the PDMS composite film fully contact with aluminum. The repeated press and release leads to the contact and separation of the triboelectric layers, enables the flow of current in the external circuit.

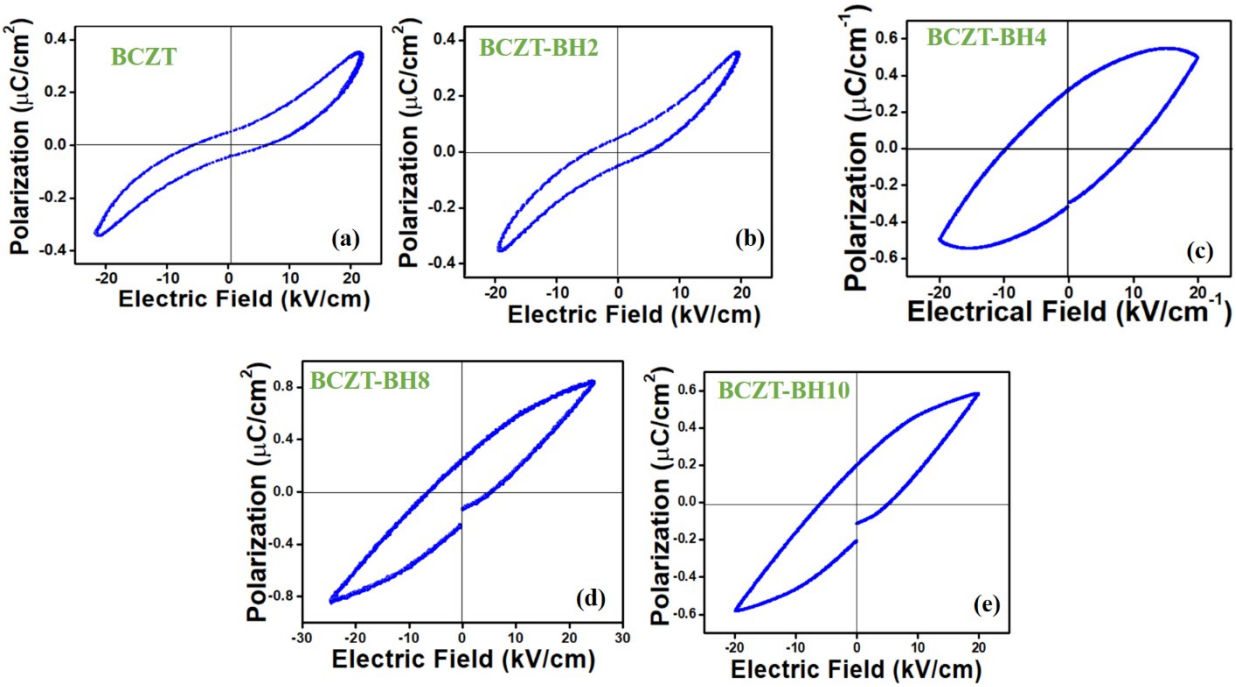

Figure S4: P-E loop of the (a) BCZT, (b) BCZT-BH2, (c) BCZT-BH4, (d) BCZT-8, (e) BCZT-BH10

Composition	Remnant Polarization (P_r)
BCZT	0.04 μC/cm^2
BCZT-BH2	0.06 μC/cm^2
BCZT-BH4	0.27 μC/cm^2
BCZT-BH6	0.70 μC/cm^2
BCZT-BH8	0.31 μC/cm^2
BCZT-BH10	0.19 μC/cm^2

Table S1: Comparison of Remnant polarization in the prepared BCZT ceramics with various doping concentrations

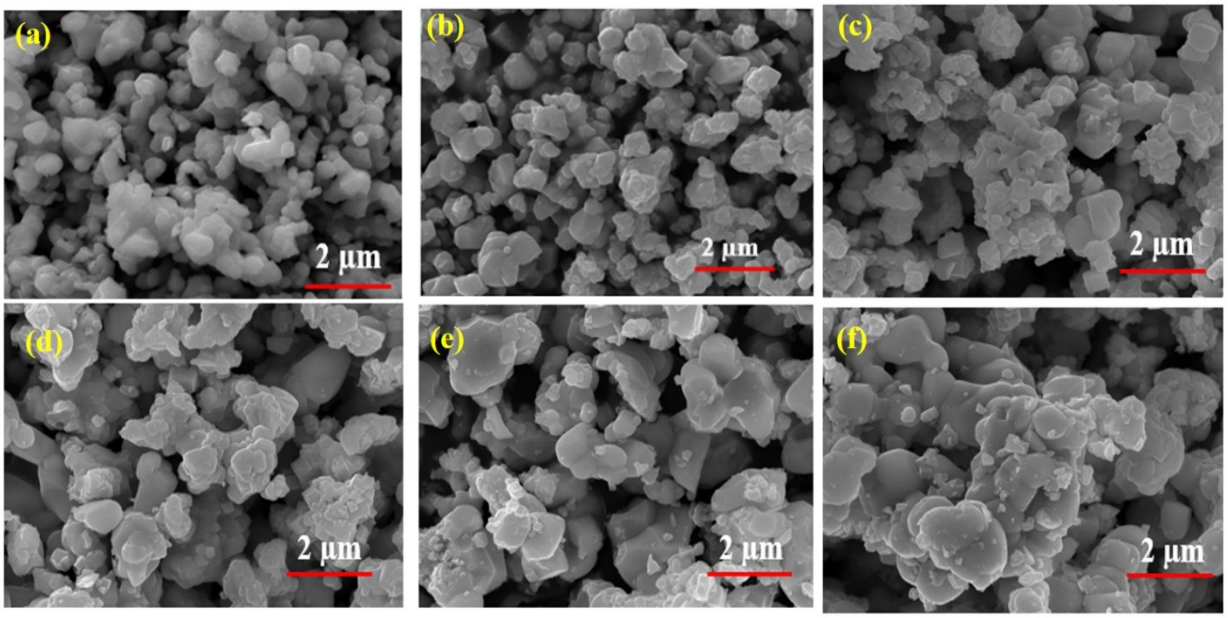

Figure S5: Surface morphology of (a) BCZT, (b) BCZT-BH2, (c) BCZT-BH4, (d) BCZT-8, (e) BCZT-BH10

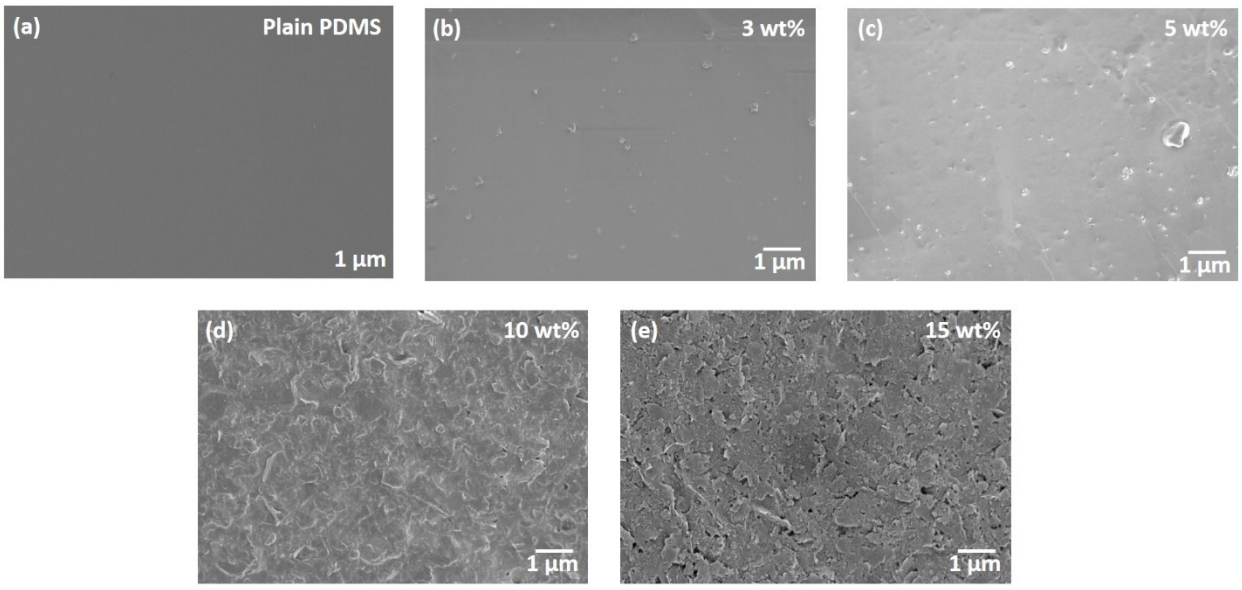

Figure S6: (a) Plain PDMS (b) 3 wt% particle loading (c) 5 wt% particle loading (d) 10 wt% particle loading and (e) 15 wt% particle loading

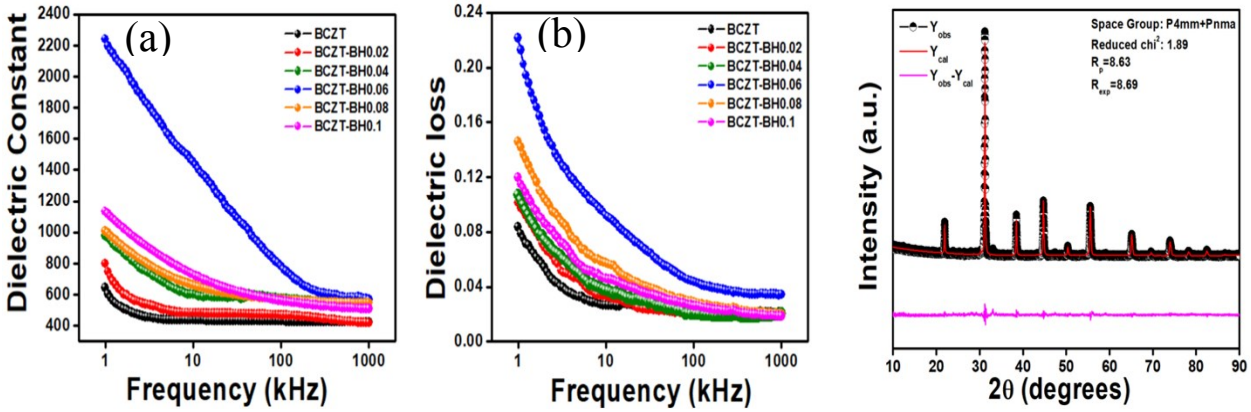

Figure S7: Frequency dependent (a) dielectric constant, (b) dielectric loss and (c) rietveld analysis of the BCZT-BH6 sample confirming the presence of combine phases (orthorhombic and tetragonal)

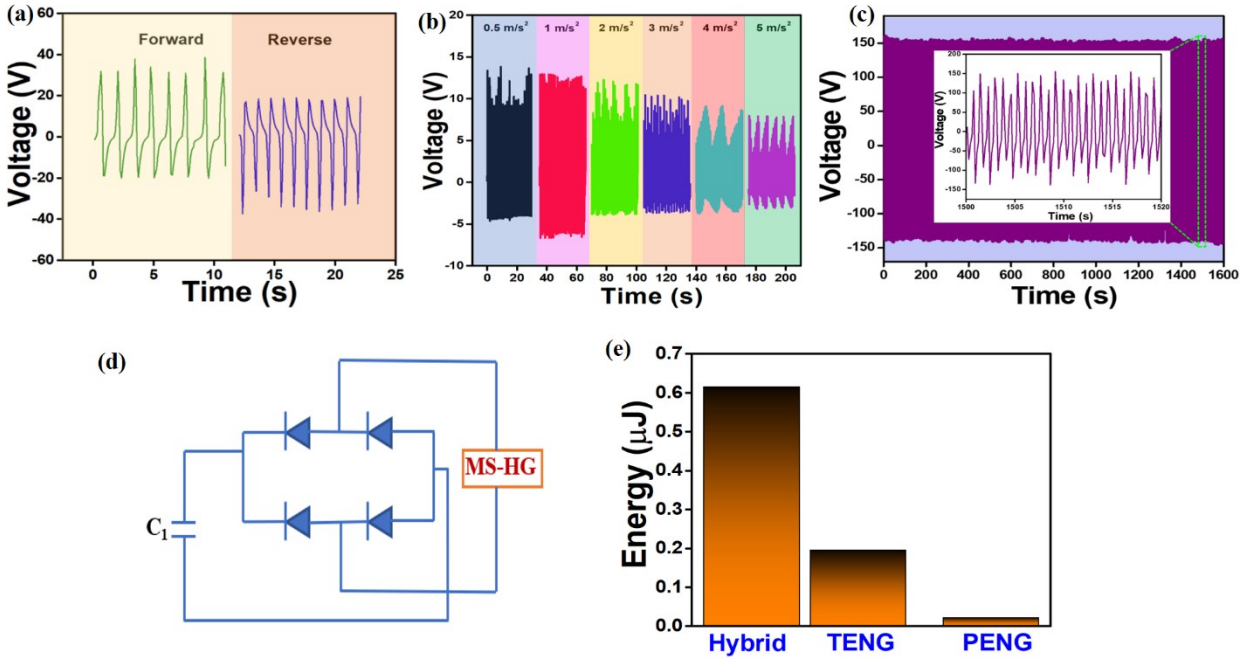

Figure S8: (a) The switching polarity test of the poled PNG-3 device, (b) The voltage output of the unpoled PNG-3 device at different acceleration, (c) The results of the operational stability test during 1600 sec of the M-HG device, (d) The equivalent circuit of the capacitor charging, (e) The energy stored by the 1 μF capacitor by PENG, TENG and hybrid device.

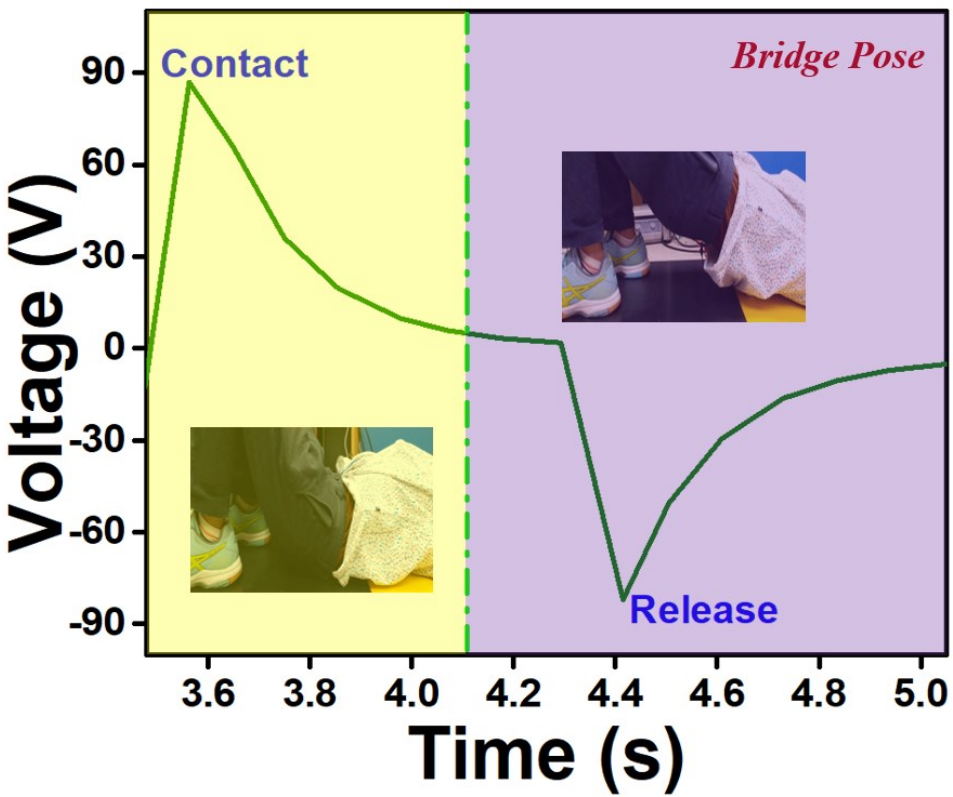

Figure S9: Voltage peak pattern of MS-HG during contact and separation upon body activity (bridge pose)